Analysis of the kinetic slowing down during carbonation of CaO by CO$_2$

Lydie Rouchon · Loïc Favergeon · Michèle Pijolat

Abstract In order to improve the capture capacity of CaO-based sorbents, it appears important to understand the mechanism of calcium oxide carbonation and to get details on kinetic law controlling the reaction, which has not been really studied up to now. To investigate this mechanism, CaO carbonation kinetics was followed by means of thermogravimetric analysis (TG) on divided materials, of textural and morphological characterisations and of an original kinetic approach devoted to look for the rate-determining step controlling the reaction rate. In order to better describe the reaction mechanism, the influence of intensive variables such as carbonation temperature and CO$_2$ partial pressure were investigated. TG curves obtained under isothermal (450–650 °C) and isobaric conditions (2–30 kPa) show a strong slowing down of the conversion leading to incomplete reaction. This slowing down and the fractional conversion at which it appears depend on carbonation temperature and CO$_2$ partial pressure. To explain these results, particular attention has been paid to the evolution of textural properties of the solid during processing. The solid powder consists of porous aggregates in which the porosity changes along the reaction due to the difference in the molar volumes of CaO and CaCO$_3$. Temperature jumps during TG experiments have put in evidence a complex kinetic behaviour since three distinct domains must be distinguished, over all the conversion range, whatever the temperature and CO$_2$ pressure could be. The discussion of the results emphasises the role of the porosity on the kinetic non-Arrhenius behaviour observed in the second domain.

L. Rouchon · L. Favergeon (✉) · M. Pijolat
École Nationale Supérieure des Mines de Saint-Étienne,
SPIN-EMSE, CNRS:FRE3312, LPMG, 158 Cours Fauriel,
42023 Saint-Étienne, Cedex 2, France
e-mail: favergeon@emse.fr

Introduction

Anthropogenic carbon dioxide (CO$_2$) emissions, major contributors to the greenhouse effect, are considered as the main cause of climate change [1]. So, decrease of CO$_2$ emitted by large industrial combustion sources or power plants is an important scientific goal. Among the various way of CO$_2$ capture, the use of sorbents like calcium oxide (CaO) has been extensively studied [2]. Indeed the reaction of carbonation of CaO with CO$_2$, which corresponds to equation R1, is considered as an important role to play in the future at an industrial scale [3].

$$CaO(s) + CO_2(g) \rightarrow CaCO_3(s) \qquad (R1)$$
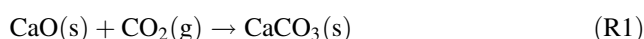
This carbonation reaction has been studied from an experimental point of view for numerous industrial processes such as CO$_2$ separation from flue gas [4, 5], chemical heat pump [6–9], energy's storage [10, 11], reaction integrated gasification process for H$_2$ production [12, 13] or sorption enhanced chemical-looping reforming for H$_2$ production [14].

Even if several studies [15–19] have been done in order to explain the decrease of the maximum extent of carbonation along carbonation/decarbonation cycles, comprehensive studies of the R1 equation remain quite rare.

To our knowledge, few authors have proposed kinetic modelling to describe the carbonation reaction. They agree on the fact that the reaction occurs by a rapid, chemically controlled initial reaction period, followed by a much slower second stage [20].

The models proposed by these authors are generally based on the shrinking core model (SCM) but the assumptions of

such a kinetic model have never been verified for this reaction. Bouquet et al. [15] directly used this SCM and Bhatia and Perlmutter [21] applied the random pore model. Both works allowed to represent experimental data for the rapid initial stage of the reaction but the kinetic slowing down and the slow second stage cannot be modelled correctly.

Lee [22] applied the SCM for both periods (chemical reaction control regime and diffusion control regime) and determined apparent activation energies in each case, but they did not model the kinetic slowing down.

Sun et al. [23] used the grain model under chemical reaction control regime to model the first rapid period. Nevertheless their approach led them to determine a kinetic parameter by considering only about 2 s of reaction. Then [24] they attempted to model the kinetic slowing down corresponding to the sudden change from the fast to the slow stage. They based their model on discrete pore size distribution measurement in order to fit experimental data.

Finally, the latest work about kinetic modelling for the CaO carbonation was done by Li et al. [25]. They wrote a rate equation assuming that the reaction proceeds by nucleation and growth of $CaCO_3$ islands at the CaO surface. Nevertheless, no experimental verification of this assumption was given.

Findings of Abanades and Alvarez [18] suggest that pore size distribution plays a crucial role for the CaO–CO_2 reaction. When the pore size distribution changes during calcination/carbonation cycles, the reactivity of the sorbent is altered accordingly.

This article aims to clearly put in evidence which are the links between the textural changes and the lowering of the carbonation reaction rate. Isothermal and isobaric conditions were used to study CaO carbonation kinetics in the range 450–650 °C and 2–30 kPa in CO_2. The article first presents the results of textural and morphological characterisations at various stages of carbonation. Then the main features of the kinetic curves obtained by thermogravimetry are reported. In the last section, the kinetic behaviour is analysed on the basis of the rate-determining step assumption whose validity can be experimentally verified [26] by means of the jump method [27, 28]. By this way, it can be shown that the kinetic modelling of CaO carbonation should involve both nucleation-growth kinetics and gaseous transfer into the aggregates porosity.

Experimental

Material

In order to study the reaction of CaO carbonation, the starting material was a $CaCO_3$ powder systematically calcinated at 800 °C under a helium flow of 2 L h^{-1}. This prevents air exposure of CaO and ensures that the surface state of the particles before carbonation is the same in all the experiments.

The starting $CaCO_3$ powder (Prolabo) has a purity of 99.5 wt%. The percentage of MgO in this material is 0.09 wt%. Impurities, such as phosphorus oxide (0.1 wt%), Fe_2O_3 (0.06 wt%), K_2O (0.06 wt%) and others (<0.08 wt%)) were also present. The $CaCO_3$ mean particle size is about 3 μm.

Kinetic measurements

The Setaram TAG 16 is a symmetrical balance able to work at temperatures up to 1,600 °C. The sample holder was a platinum crucible. The reacting gas mixture contained CO_2, He and water vapour in various proportions fixed due to mass flow controllers and a steam generator (Setaram Wetsys). Water vapour partial pressure is known to significantly enhance the reaction rate [29]. So, we decided to maintain it at 0.2 kPa in all our experiments.

For each experiment, around 10 mg of $CaCO_3$ was loaded in a platinum crucible which represents a powder bed of about 1.5 mm height. First, vacuum up to 10^{-6} Pa was made in the thermogravimetric analyser. A complete calcination at 800 °C during 1 h under dry He (total flow rate: 2 L h^{-1}) was realised in order to completely decompose $CaCO_3$ into CaO. The temperature was then decreased at 20 °C min^{-1} to the carbonation temperature, in the range 450–650 °C, and stabilized during around 10 min before introducing the carbonation gas mixture (CO_2/He/ H_2O) with a total flow rate of 2 L h^{-1}. For thermogravimetric measurements, the time necessary to reach $\approx$90 % of $P(CO_2)$ after its introduction was determined due to a mass spectrometer (Pfeiffer vacuum ThermoStar) and is equal to about 3 min. The whole procedure is summarised in Fig. 1 which represents the mass and temperature change during a typical experiment with 10 mg of sample
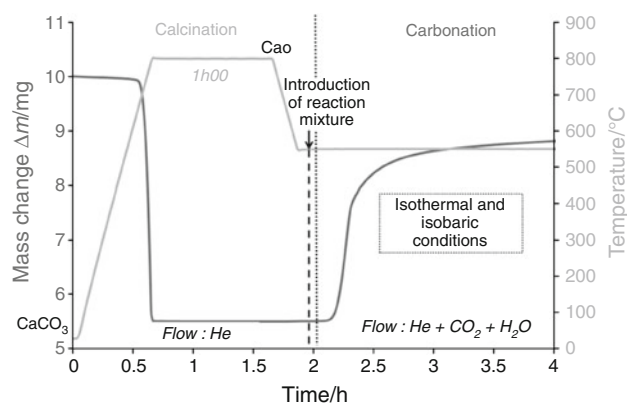

Fig. 1 Protocol of an experiment on TG or tube furnace (temperatures and gas flow) and typical shape of carbonation curves (carbonation at 550 °C under 5 kPa in CO_2 of 50 mbar and 0.2 kPa in water vapour)

(it has been experimentally verified that this initial sample mass is low enough to be sure that heat and mass transfers inside the granular medium can be neglected).

By this way, we performed carbonation reaction under isothermal and isobaric conditions for CO_2 partial pressure in the range 2–5 kPa.

Plots of fractional conversion α versus time were obtained from the measured mass changes according to:

$$\alpha = \frac{m - m_0}{\Delta m_{th}} = \frac{\Delta m}{\Delta m_{th}} \quad (1)$$

with m the sample mass at the time t, m_0 the sample mass of CaO just before carbonation and Δm_{th} the theoretical mass gain given by:

$$\Delta m_{th} = \frac{m_0}{M_{CaO}} M_{CO_2} \quad (2)$$

with M_{CaO} the molar mass of CaO, equal to 56 g mol^{-1} and M_{CO_2} the molar mass of CO_2 equal to 44 g mol^{-1}.

Samples characterisations

In order to obtain a sufficient amount of sample to allow measurements of specific surface area thanks to BET analysis, a Carbolite CTF 15 75 610 tube furnace was used. It consisted of an alumina tube heater (70 mm diameter and 1,430 mm length), heating resistors and a temperature programmer. It was also equipped with a primary vane pump to make vacuum into the tube prior to introducing a controlled atmosphere of CO_2, He and H_2O. We used an alumina sample holder. The sample mass was measured before and after each experiment, with a balance Precisa XR 305A. For each experiment, about 4 g of $CaCO_3$ was loaded in the crucible. The procedure used for calcination and carbonation in the tube furnace was the same as for thermogravimetric analysis (TG) experiments, except that the total flow rate was 24 L h^{-1} in order to assure the same flow velocity around the powder (i.e. about 0.173 cm s^{-1}). The temperature is controlled using a thermocouple placed near the sample allowing to make the reaction in much closed way in both the furnace and the thermobalance. For each experiment, the sample was weighted before and after the reaction and the fractional conversion was calculated using Eq. (1).

Decarbonated and carbonated samples were studied by means of a scanning electron microscope (SEM) JEOL JSM6400. Samples were put on a graphite adhesive tab placed on an aluminium sampler and coated with a thin film (≈ 20 nm thick) of gold.

The specific surface area of initial CaO and partially carbonated samples were measured by means of the Brunauer-Emmett-Teller (BET) and the α_s methods [30]. The BET method allows the determination of the specific surface area due to mesopores (2 nm $< d <$ 50 nm) whereas the α_s method gives access to both mesoporous and microporous ($d < 2$ nm) surfaces. The pore size distribution was determined by means of the Barrett-Joyner-Halenda (BJH) method. Specific surface area and pore size distribution ware obtained using a Micromeritics ASAP 2000 analyser with nitrogen.

Results and discussion

Characterisation of initial CaO powder (after $CaCO_3$ decomposition)

The specific surface area of a CaO sample after calcination at 800 °C under dry helium flow in the tube furnace CTF 15 75 610 was equal to 8 m^2 g^{-1}. The equivalent spherical diameter d was obtained from Eq. 3:

$$d = \frac{6}{\rho \cdot S} \quad (3)$$

where ρ is the CaO volumic mass, equal to 3.3 g cm^{-3} and S the specific surface area. According to Eq. 3, d is around 0.23 μm.

Scanning electron microscopy was also used to observe the starting CaO powder. Results are shown in Fig. 2a–c. It is clear that the initial CaO powder consists of facetted porous aggregates of dense 1–3 μm particles as indicated by particle size analysis (Laser granulometer, Mastersizer 2000), not shown here. The size of the aggregates varies from 10 to 50 μm.

Kinetic curves

Figure 3 presents the fractional conversion versus time for CaO carbonated with 5 kPa of CO_2, at different carbonation temperatures ranging from 450 °C to 650 °C. Effect of CO_2 partial pressure was also studied at 650 °C from 2 to 30 kPa. Results are shown in Fig. 4a, b. Kinetic curves of both Figs. 3 and 4 exhibit a similar shape which can be divided into three stages: first an induction period, then a very fast carbonation stage up to a breakpoint and finally a sluggish stage up to the end. Besides total conversion ($\alpha = 1$) is never reached.

The duration of the induction period (τ) depends on the CO_2 partial pressure and temperature. Its measurement can be done by considering the time elapsed from the CO_2 partial pressure establishment (3 min after CO_2 introduction) until the mass gain began to be greater than the thermobalance noise ($\Delta m > 1$ μg). Depending on T and $P(CO_2)$ conditions, τ can be as long as 20 min.

Figure 5a, b represent the variation of the induction period τ with the carbonation temperature and CO_2 partial
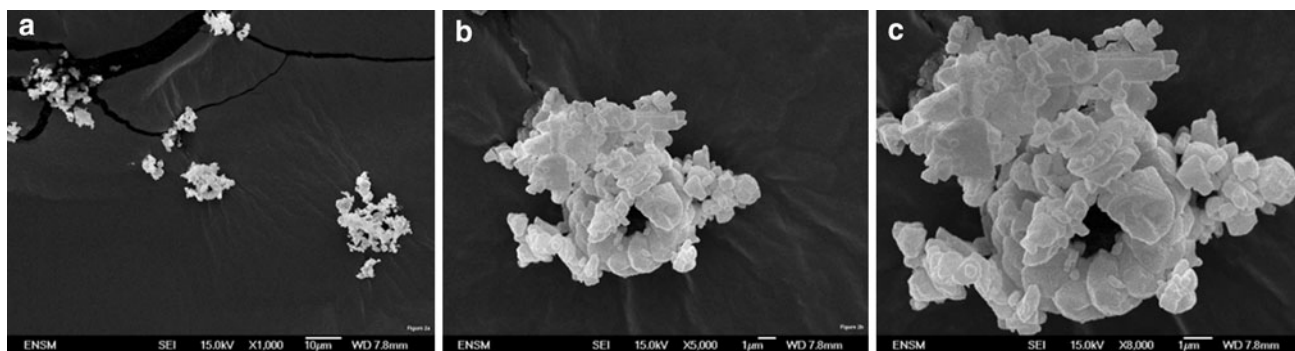
Fig. 2 SEM images of sample of CaO obtained from CaCO₃ for 1 h 00 at 800 °C under He flow in TG **a** ×100; **b** ×5,000; **c** ×8,000
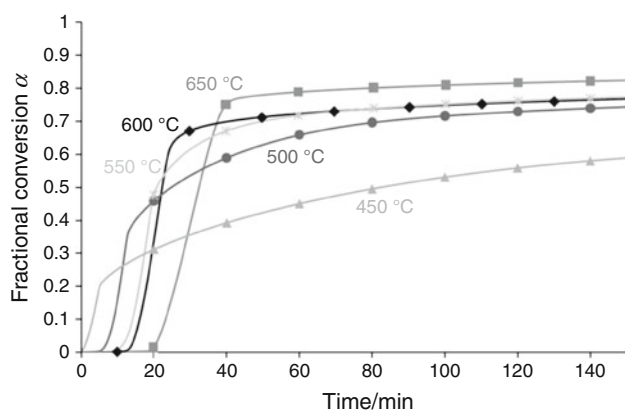

Fig. 3 Isothermal kinetic curves of CaO carbonation under a CO_2 partial pressure of 5 kPa and water vapour partial pressure of 0.2 kPa

In Fig. 6, the values of α at the breakpoint α_d (when the strong slowing down occurs) obtained from the α(t) curves of Figs. 3 and 4 have been plotted. These values have been determined at various carbonation temperatures and various CO_2 partial pressures. The plot of Fig. 6a shows that α_d increases linearly with carbonation temperature. However, α_d does not vary significantly with CO_2 partial pressure (Fig. 6b). It can be noticed that the dependence of τ and α_d with temperature are very similar, and that they are practically constant over 5 kPa.

On the origins of the kinetic blocking

Textural and morphological changes

CaO samples were carbonated up to various fractional conversions between 0 and 0.7 in the tube furnace at 550 and 450 °C under 5 kPa of CO_2. The values of the specific surface area as a function of the fractional conversion are shown in Fig. 7. At the beginning, the specific surface areas of the samples were found to remain around 8 m² g⁻¹. Then a decrease occurs for a fractional conversion which depends on the carbonation temperature, the

pressure, respectively. It can be seen that the induction period τ increases quite linearly from ∼0 to 20 min with carbonation temperature in the range 450–650 °C (Fig. 5a). An increase in CO_2 pressure from 2 to 5 kPa provokes a large drop in the induction time at 650 °C from 135 to 20 min, whereas from 5 to 30 kPa, it decreases only to 19 min.
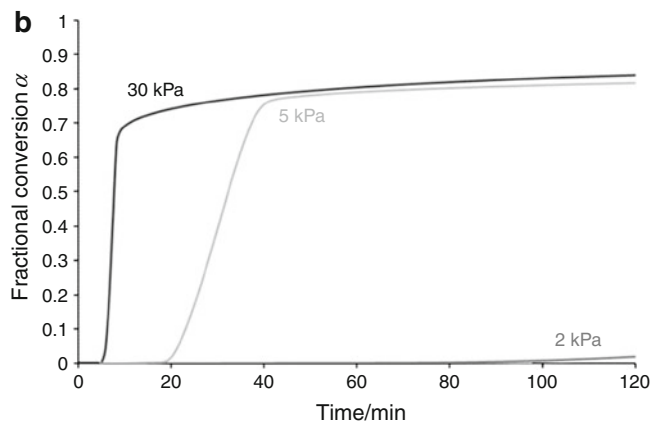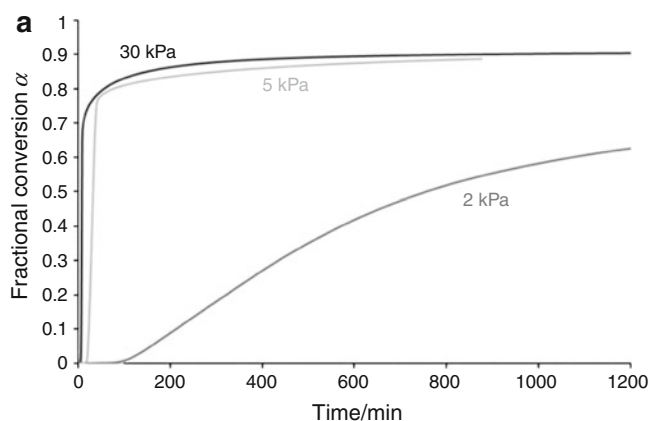

Fig. 4 Isobaric kinetic curves of CaO carbonation at 650 °C (water vapour partial pressure of 0.2 kPa): **a** between 0 and 1,200 min; **b** between 0 and 100 min
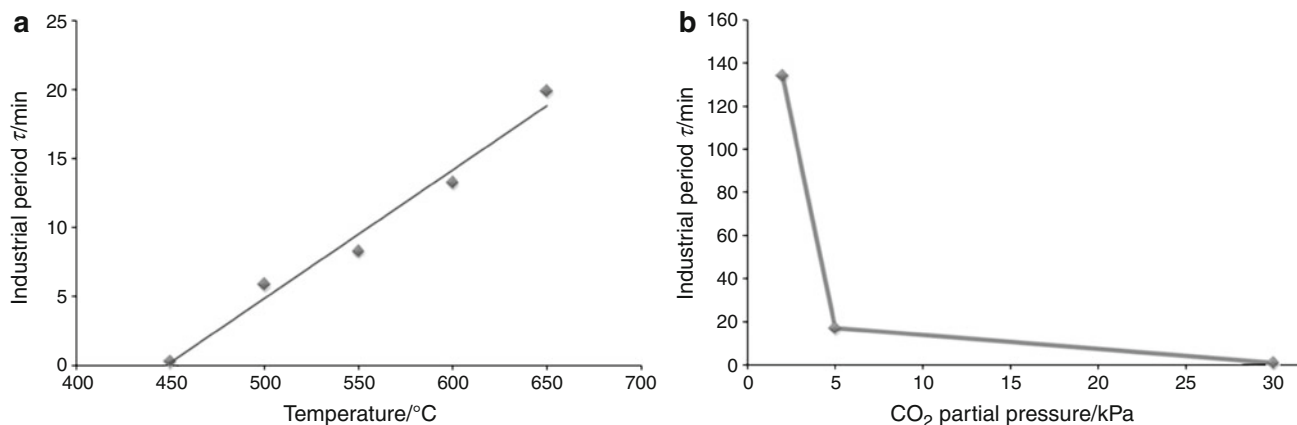
Fig. 5 Evolution of induction period τ **a** with carbonation temperature ($P_{CO_2} = 5$ kPa) and **b** with CO_2 partial pressure ($T = 650$ °C)
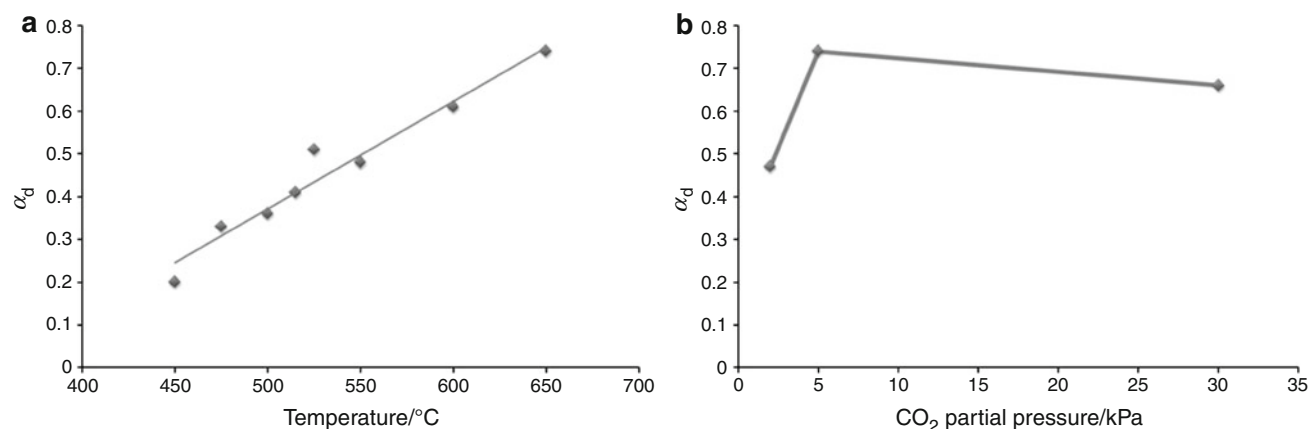

Fig. 6 Evolution of fractional conversion α_d **a** with carbonation temperature ($P_{CO_2} = 5$ kPa) and **b** with CO_2 partial pressure ($T = 650$ °C)

lower temperature and the higher fractional conversion. However, it is clear that the conversion at which the decrease in the specific surface area begins does not correspond to the α_d values which were observed in the same temperature and CO_2 pressure conditions (vertical dotted lines in Fig. 7). It can, therefore, be inferred that the loss in specific surface area is not directly responsible for the strong slowing down of the reaction.

In order to observe the morphological changes at the particle and aggregate scales during carbonation, scanning electron microscopy was also used. Figure 8a–e show the aggregate surface of carbonated samples at various fractional conversions: 0.05, 0.19, 0.36, 0.63, and 0.8 (b–e). As far as the fractional conversion increases, the size of the dense particles increases and the porosity between them tends to disappear. Such changes are not surprising since the volume expansion due to the CaO–$CaCO_3$ transformation is quite important (the ratio of the molar volumes $CaCO_3$/CaO is equal to 2.13). For spherical particles if the initial radius is equal to 1 μm, the final radius must reach 1.28 μm when CaO is totally transformed into $CaCO_3$. This

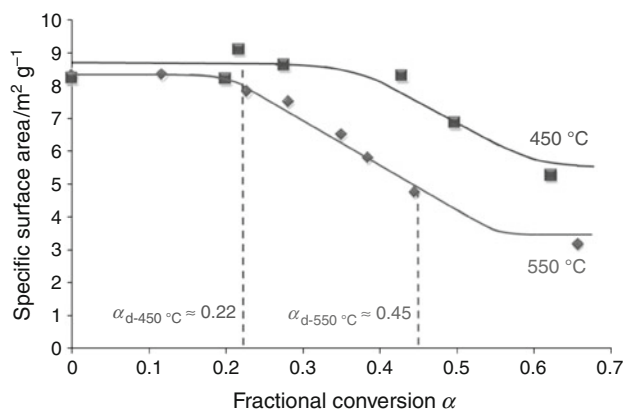**Fig. 7** Change in specific surface area versus fractional conversion for sample carbonated at 550 *filled square* and 450 °C *filled diamond* under 5 kPa of CO_2

decrease in the porosity when the reaction proceeds is confirmed by the pore size distributions obtained by the BJH method at various fractional conversions for samples
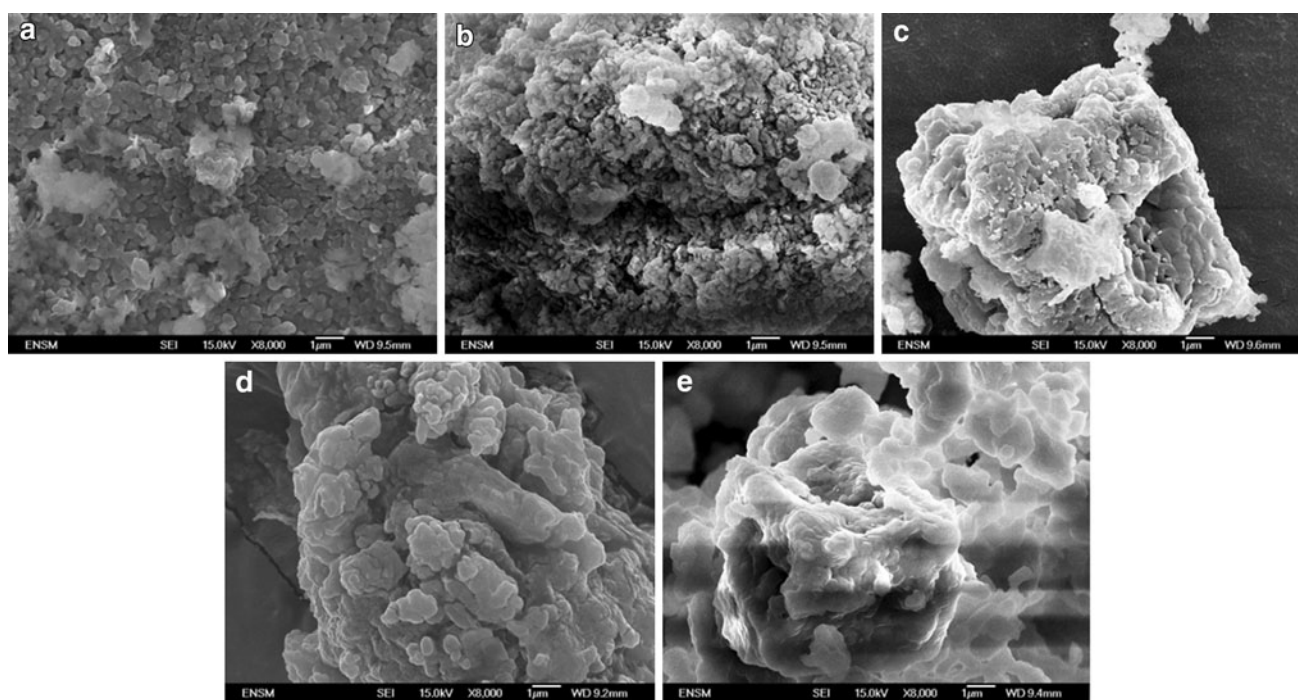
Fig. 8 SEM image of samples carbonated (550 °C; 5 kPa of CO_2) at different fractional conversions **a** 0.05, **b** 0.19, **c** 0.36, **d** 0.63 and **e** 0.8

carbonated at 550 °C under $P(CO_2) = 5$ kPa as shown in Fig. 9.

Thus at the aggregate scale, the decrease in the mean pore size and the subsequent loss in porosity (as it can be seen in Fig. 8e) at least at the outermost layers of the aggregates are very probably involved in the slowing down of the reaction rate observed in the $\alpha(t)$ curves.

The problem which remains at this stage of the study is to understand how these morphological changes may have an effect on the kinetic behaviour of the carbonation reaction. In the next section, special attention will be paid to the rate-determining step of the carbonation reaction since to our knowledge such kinetic aspects have not yet been really investigated.

Kinetic rate-controlling changes

The study of the kinetic curves has pointed out the existence of an induction time whose duration depends on the temperature and CO_2 partial pressure. Such a behaviour suggests that the nucleation is not instantaneous.

Usual heterogeneous kinetic models are based on several assumptions: (i) experimental conditions must allow the establishment of a steady state, (ii) the growth rate of the product phase is controlled by one elementary step called the rate-determining step and (iii) then geometrical assumptions such as the particle shape, the location of the rate-determining step and the sense of development of the product phase have also to be considered in order to
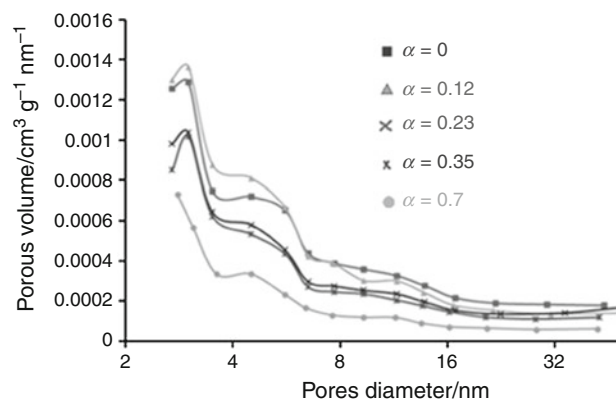

Fig. 9 Pore size distribution obtained by the BJH method for different fractional conversions (carbonation at $T = 550$ °C and $P(CO_2) = 5$ kPa)

calculate the expression of the reaction rate. In addition most of authors also suppose that this rate follows the Arrhenius law, but it is not necessary to make a restrictive assumption for the analysis of isothermal and isobaric kinetic data [31]. Finally, assumptions (i) and (ii) allow expressing the reaction rate $d\alpha/dt$ according to Eq. (4) [31, 32].

$$\frac{d\alpha}{dt} = \phi(T, P_i, \ldots)S_m(t) \tag{4}$$

where $\phi(T, P_i, \ldots)$ is the areic rate of growth (in mol m^{-2} s^{-1}) which we used to call 'areic growth reactivity' and which depends only on the thermodynamic

variables, and the molar space function $S_m(t)$ is a function of time (expressed in $m^2\ mol^{-1}$) and is related to the extent reaction area where the rate-determining step of growth takes place. Combining appropriate (iii) assumptions provides equations leading to the expression of $S_m(t)$ which can be reduced to a function of α in some limiting cases as for example instantaneous nucleation [33]. Here, the carbonation of CaO involves both nucleation and growth, so in the following we will use Eq. (4).

It was previously shown that using an experimental test which we will call here the 'ϕS_m' test [26] allows to validate that the reaction rate follows Eq. (4) in the range of α between 0 and 1. The test is based on the jump method [27, 28], which consists in a sudden change of a thermodynamic variable (gas partial pressure or temperature) from a value Y_0 to a value Y_1, at a given time t_i (α_i at t_i). Let $(d\alpha/dt)_{bi}(Y_0)$ and $(d\alpha/dt)_{ai}(Y_1)$ be the rates before and after the sudden change at the fractional conversion α_i, respectively. According to Eq. (4) the ratio R of both rates is given by:

$$R = \frac{(d\alpha/dt)_{ai}(Y_1)}{(d\alpha/dt)_{bi}(Y_0)} = \frac{\phi(Y_1)S_m(t_i)}{\phi(Y_0)S_m(t_i)} = \frac{\phi(Y_1)}{\phi(Y_0)} \tag{5}$$

So, the ratio of the rates before/after the jump must remain constant, when the 'ϕS_m test' (assumption (ii)) is verified whatever the time t_i or the fractional conversion α_i at which the jump is done. It is, however, necessary that the sudden jump should be very fast relative to the variation of the rate with time otherwise it could not be possible to eliminate the $S_m(t)$ terms in the ratio of Eq. (5).

In the present case, the jump method was applied during an experiment started at T_0 by increasing quickly (30 °C min^{-1}) the carbonation temperature from T_0 to a value $T_1 = T_0 + 15$ °C. We performed the 'ϕS_m test' in several temperature conditions, the initial temperature T_0 being equal to 450, 475, 500, 525 and 550 °C, and the CO_2 partial pressure being equal to 5 kPa.

The results of experiments done with 5 kPa of CO_2 are shown in Fig. 10a. One can see that whatever the initial temperature could be, the ratio of the rates after to before the temperature jump is not constant over all the fractional conversion range from 0 to 1. In fact, one can distinguish three different domains as shown in Fig. 10b: the domain I where the ratio seems to remain constant, the domain II where the ratio strongly decreases until a minimum value R_{min} (which corresponds to a fractional conversion $\alpha(R_{min})$) and finally the domain III where the ratio reaches another constant value. Thus it can be inferred that there does not exist a single rate-determining step over all the range of α between 0 and 1. The fact that the 'ϕS_m' test may be considered as validated in domains I and III (R value constant in both domain) indicates that the kinetics of the reaction may be reasonably described by Eq. (4), but the values of R being different, functions ϕ are very probably

different in domains I and III. Concerning domain II, it can be seen from Fig. 10 that most of the values of R obtained in this domain are lower than 1 which traduces the fact that an increase of carbonation temperature of 15 °C has a inhibiting effect (non-Arrhenius behaviour), since $R < 1$ means that the growth rate at T_1 is lower than those at T_0. In order to explain this non-Arrhenius behaviour, it is important to focus on the thermodynamics aspects of the reaction, especially the deviation of the experimental conditions from the equilibrium ones.

From the induction time, it is know that the reaction proceeds due to nucleation and growth processes. As far as the growth process is concerned, the carbonation mechanism may be decomposed into a sequence of elementary steps (adsorption, interfacial reactions and diffusion).

Without entering in the details of the elementary steps involved in the carbonation growth process, a simple way of representing the adsorption or interfacial steps is as follows:

$$\sum \beta_j X_j \leftrightarrow \sum \beta_k X_k \tag{6}$$

where X_j and X_k may be intermediate species and β_j and β_k the corresponding stoichiometric number, which is also the kinetic order respective to the intermediate. Thus, if reaction (6) is supposed to be the rate-determining step of the growth process, the areic reactivity of growth for the reaction may be expressed by Eq. (7):

$$\phi = k_i \prod [X_j]^{\beta_j} - k_i' \prod [X_k]^{\beta_k} \tag{7}$$

where k_i is the kinetic constant of step i and k_i' the kinetic constant of the inverse step. Equation (7) may be rearranged into (8):

$$\phi = k_i \prod [X_j]^{\beta_j} \left(1 - \frac{\frac{\prod [X_k]^{\beta_k}}{\prod [X_j]^{\beta_j}}}{\frac{k_i}{k_i'}} \right) \tag{8}$$

If the rate-determining step is a diffusion of an intermediate species Y, then the areic reactivity of growth is given by:

$$\phi = D_Y \frac{\Delta C_Y}{l_0} \tag{9}$$

where D_Y is the diffusion coefficient of Y, ΔC_Y is the difference in the concentrations in Y at both sides of the diffusion layer, and l_0 is a length taken equal to 1 m in order to respect the unity of ϕ (in mol $m^2\ s^{-1}$) [32]. Then, as in homogeneous kinetics, the fact that one of the elementary steps of the mechanism is supposed to be the rate-determining step, implies that all the other steps are at equilibrium (in case of a diffusion, it comes $\Delta C_Y = 0$). This provides a set of equations whose unknown quantities are the concentrations of the intermediate species.
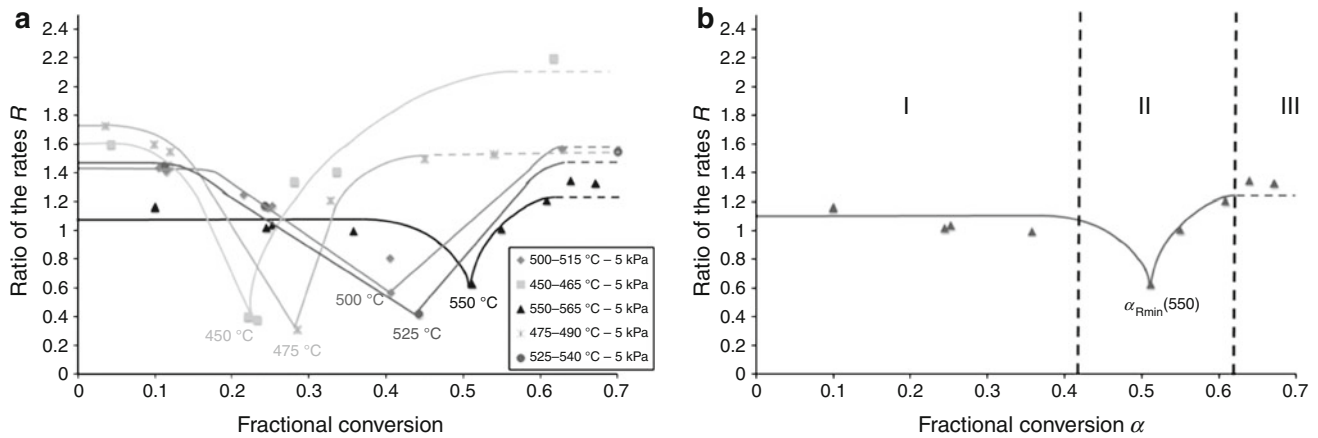
Fig. 10 a Results of 'ϕS_m test' experiments at 5 kPa of CO_2 for T_0 equal to 450, 475, 500, 525 and 550 °C; **b** illustration of three separate domains at 550 °C

In general such a system of simultaneous equations may be solved leading to the final expression of ϕ [32]:

$$\phi = k_i \prod [X_j]^{\beta_j} \left(1 - \left[\frac{P_{CO_2}^{eq}}{P_{CO_2}^{exp}}\right]^{1/\lambda}\right) \quad (10)$$

in which the term into brackets represents the deviation from equilibrium where $P_{CO_2}^{exp}$ represents the experimental CO_2 partial pressure and $P_{CO_2}^{eq}$ represents the equilibrium one; $P_{CO_2}^{eq}$ is determined by the opposite of the equilibrium constant of the overall reaction and depends on temperature only; λ is a positive number which depends only on the elementary steps of the mechanism sequence since a linear combination of them should give back to the global carbonation reaction balance.

Combining Eqs. (5) and (10), the expression of the ratio R corresponding to a temperature jump becomes:

$$R = \frac{\left(k_i \prod [X_j]^{\beta_j}\right)_a}{\left(k_i \prod [X_j]^{\beta_j}\right)_b} \frac{\left(1 - \left[\frac{\left(P_{CO_2}^{eq}\right)_a}{P_{CO_2}^{exp}}\right]^{1/\lambda}\right)}{\left(1 - \left[\frac{\left(P_{CO_2}^{eq}\right)_b}{P_{CO_2}^{exp}}\right]^{1/\lambda}\right)} \quad (11)$$

where $\left(P_{CO_2}^{eq}\right)_a$ and $\left(P_{CO_2}^{eq}\right)_b$ correspond to the equilibrium CO_2 partial pressure after and before the jump, respectively.

In fact, $P_{CO_2}^{eq}$ values after and before the temperature jump are fixed by the experimental temperature and with a low sample mass in the crucible, the temperature is assumed to be the same in all parts of the powder. Thus the decrease of R to values less than 1 can be attributed to CO_2 pressure gradients inside the aggregates porosity. This is illustrated by Fig. 11a, b which represent $P_{CO_2}^{eq}$ versus

temperature curve for CaO carbonation confronted to $P_{CO_2}^{exp}$ at the entrance and at the bottom of a pore. It is clear that the situation encountered for CaO particles located in the periphery of the aggregates may be very different from that occurring inside the aggregate core. Figure 11a shows that in the first case (outside) $P_{CO_2}^{exp}$ is fixed by the experimental conditions in the gas flow of the thermobalance. Inside the aggregate pores, $P_{CO_2}^{exp}$ is expected to decrease progressively as far as time and depth increase due to CO_2 consumption by the reaction. Before the temperature jump, $P_{CO_2}^{exp}$ inside a pore is thus nearer to the equilibrium curve than $P_{CO_2}^{exp}$ outside and reach almost the $\left(P_{CO_2}^{eq}\right)_a$ value after the jump. So, the ratio $\left(P_{CO_2}^{eq}\right)_a / \left(P_{CO_2}^{exp}\right)$ will increase.

In the case where $P_{CO_2}^{exp}$ is very close to $P_{CO_2}^{eq}$ (at the bottom of a pore), we calculated the first term of the product in the right hand side of Eq. (11) by considering $\lambda = 1$. Values of the different terms of Eq. (11) are summarised in Table 1 for R_{min} determined at each temperature jump. The results of Table 1 show that the term $\frac{\left(k_i \prod [X_j]^{\beta_j}\right)_a}{\left(k_i \prod [X_j]^{\beta_j}\right)_b}$ is always higher than 1 for all the jumps in various conditions of temperatures.

So, values of R lower than 1 must imply that the second term of the product verifies the following condition:

$$1 - \left(\frac{\left(P_{CO_2}^{eq}\right)_a}{P_{CO_2}^{exp}}\right)^{1/\lambda} < 1 - \left(\frac{\left(P_{CO_2}^{eq}\right)_b}{P_{CO_2}^{exp}}\right)^{1/\lambda} \quad (12)$$

and, in consequence, the value of $\left(P_{CO_2}^{eq}\right)_a / \left(P_{CO_2}^{exp}\right)$ must not be very far from 1.

The inequality of Eq. (12) would be satisfied in the case at the bottom of a pore and leading to a decrease in R at values lower than 1.
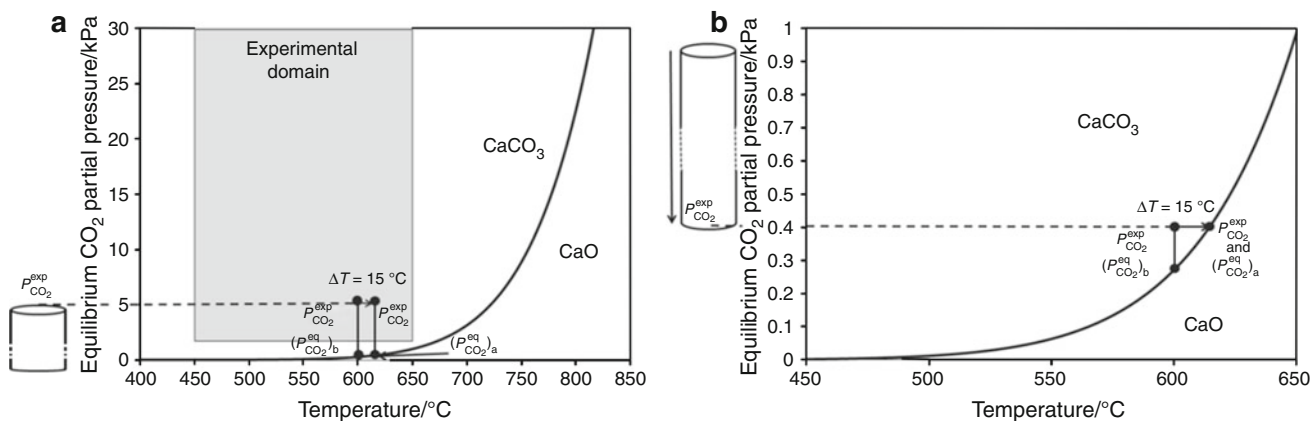
Fig. 11 $P_{CO_2}^{eq}$ versus temperature curve for CaO carbonation confronted to the $P_{CO_2}^{exp}$ at the entrance (**a**) and at the bottom (**b**) of a pore

Table 1 Calculation of the terms of Eq. (11)

Temperature jumps/°C	$P_{CO_2}^{exp}$/kPa	$\alpha(R_{min})$	R_{min}	$\dfrac{\left(1-\left[\dfrac{\left(P_{CO_2}^{eq}\right)_a}{P_{CO_2}^{exp}}\right]\right)}{\left(1-\left[\dfrac{\left(P_{CO_2}^{eq}\right)_b}{P_{CO_2}^{exp}}\right]\right)}$	$\dfrac{\left(k_i \prod [X_j]^{\beta_j}\right)_a}{\left(k_i \prod [X_j]^{\beta_j}\right)_b}$
450–465	0.0031	0.221	0.4	0.09091	4.18
475–490	0.0081	0.285	0.31	0.03226	9.61
500–515	0.021	0.406	0.57	0.1111	5.13
525–540	0.047	0.443	0.42	0.05263	7.98
550–565	0.11	0.511	0.63	0.2174	2.9

Obviously, this is a qualitative and over simplified description of what really occurs at the aggregate scale. Both CO_2 transport and CO_2 consumption, as well as possible, and gradient temperatures due to the exothermicity of the reaction (-179 kJ mol^{-1}) should be considered with spatial and time variables, in order to get a quantitative validation of all the phenomena.

Concerning the domain I, it can be considered that the kinetics, which is controlled by an elementary step, does not suffer from CO_2 pressure gradients through the aggregates, so this domain would allow to study the model of transformation at the scale of the dense particles.

In the third domain, however, the rate-determining step should be different. A possible explanation could be the closure of porosity at the periphery of the aggregates leading to a dense $CaCO_3$ shell (whose dimensions are of the order of the aggregate ones) preventing CO_2 gaseous transport.

Finally, in order to confirm that the decrease in the specific surface area is not entirely responsible for the strong kinetic slowing down previously highlighted, the values of α_d and α_{Rmin} have been plotted as a function of carbonation temperature in Fig. 12. One can see that the values of both
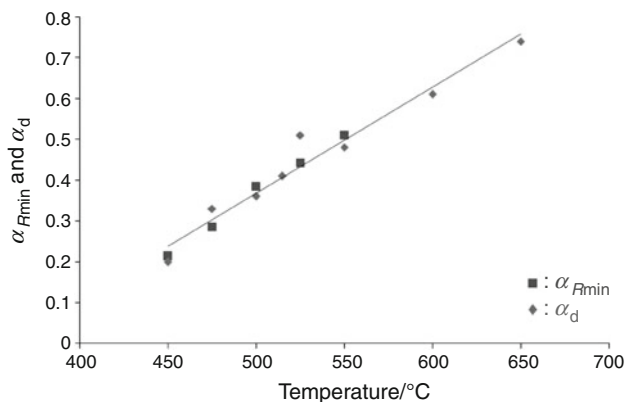

Fig. 12 Comparison between α_d and α_{Rmin} versus temperature of carbonation

fractional conversions are very similar and yet α_{Rmin} is known to vary with pressure and temperature conditions only since it is related to the $\phi(T, P)$ function only. It is interesting (cf. 'ϕS_m test' in 'Kinetic rate-controlling changes' section) to notice that the jump experiments allow to put in evidence kinetic changes due to the thermodynamic variables (such as temperature and/or pressure) which may in turn be affected

by morphological variables (such as porosity in the present study, cracks…). Besides, if decrease of specific area had been entirely responsible of kinetic brake, there would only affect the space function S_m in Eq. 4. But 'ϕS_m test' allowed us to put in evidence an effect on areic growth reactivity ϕ.

About the induction period

The induction period τ is linked to the nuclei formation mechanism, and it is well known that temperature influences the nucleation kinetics. Unfortunately nucleation mechanisms were not extensively studied and very few quantitative data can be found in literature. In a previous study [34] about dehydration of $Li_2SO_4 \cdot H_2O$, it was possible to measure the induction period for each single crystal and to determine a relation between this induction period and an areic frequency of nucleation (expressed in number of nuclei $m^{-2}\ s^{-1}$). In a study about reduction by hydrogen of U_3O_8 into UO_2, Brun et al. [35] have shown that the areic frequency of nucleation can follow a non monotonous evolution versus temperature (with a presence of a maximum) which can explain why the induction period increases when the temperature increases. Moreover, in the case of the allotropic transformation of white tin (or beta-tin) into grey tin (or alpha-tin), known as the tin pest phenomenon, the experimental results obtained by Burgers and Groen [36] indicate that the induction period increases when temperature increases from -40 to -15 °C. In the present case, we have shown in 'On the origins of the kinetic blocking' section a non-Arrhenius effect on the growth process explained by approaching equilibrium conditions into the pores due to increasing pressure gradients. It is possible to consider a similar behaviour for nucleation process which leads to a disadvantaged nucleation kinetics when temperature increases.

Conclusions

A complex behaviour of CaO carbonation kinetics has been put in evidence from thermogravimetric experiments in isothermal and isobaric conditions. Though the detailed mechanisms at the grain scale have not yet been investigated, a comprehensive study of the process occurring at porous aggregates scale has been performed due to the 'ϕS_m test' based on temperature jumps during the reaction. Over the entire range of fractional conversion α, the reaction was shown to pass through three distinct kinetic domains leading to the major following conclusions:

1- First, the reaction begins at the grain scale with a rate-determining step dominating in all parts of the aggregates; the corresponding range of conversion degree varies from 0–0.15 to 0–0.4 when the temperature increases from 450 to 550 °C;

2- The reaction follows an non-Arrhenius behaviour in the intermediate α range, explained by approaching the CaO–$CaCO_3$ equilibrium conditions into the pores due to increasing pressure gradients as far as the reaction proceeds;

3- In the last domain, another rate-determining step governs the kinetic behaviour, which could be due to porosity closure at the periphery of the aggregates; at this time, diffusion through a dense $CaCO_3$ shell around the aggregates should be involved, as proposed by Mess et al. [37].

Finally, the decrease in surface area generally involved for explaining the loss in CO_2 capture capacity of CaO powders must be seen much more as a consequence of the overall process rather than its cause.

References

1. Gray ML, Soong Y, Champagne KJ, Pennline H, Baltrus JP, Stevens RW Jr, Khatri R, Chuang SSC, Filburn T. Improved immobilized carbon dioxide capture solvents. Fuel Process Technol. 2005;86:1449–55.
2. Stanmore BR, Gilot P. Review—calcinations and carbonation of limestone during thermal cycling for CO_2 sequestration. Fuel Process Technol. 2005;86:1707–43.
3. Chrissafis K. Multicyclic study on the carbonation of CaO using different limestones. J Therm Anal Calorim. 2007;89:525–9.
4. Gupta H, Fan LS. Carbonation–calcination cycle using high reactivity calcium oxide for carbon dioxide separation from flue gas. Ind Eng Chem Res. 2002;41:4035–42.
5. Mofarahi M, Roohi P, Farshadpoor F. Study of CaO sorbent for CO_2 capture from flue gases. Vol. 17. In: 9th International Conference on Chemical and Process Engineering, Chemical Engineering Transactions; 2009. p. 403–8.
6. Kato Y, Saku D, Harada N, Yoshizawa Y. Utilization of high temperature heat using a calcium oxide lead oxide carbon dioxide chemical heat pump. J Chem Eng Jpn. 1997;30:1013–9.
7. Kato Y, Yamada M, Kanie T, Yoshizawa Y. Calcium oxide/carbon dioxide reactivity in a packed bed reactor of a chemical heat pump for high-temperature gas reactors. Nucl Eng Des. 2001;210:1–8.
8. Li G, Kanie T, Kato Y, Yoshizawa Y. Heat and mass transfer in a packed bed reactor for calcium oxide/carbon dioxide chemical heat pump. J Chem Eng Jpn. 2002;35:886–92.
9. Aihara M, Nagai T, Matsusita J, Negishi Y, Ohya H. Development of porous solid reactant for thermal-energy storage and temperature upgrade using carbonation/decarbonation reaction. Appl Energy. 2001;69:225–38.
10. Kyaw K, Matsuda H, Hasatani M. Applicability of carbonation decarbonation reactions to high-temperature thermal energy storage and temperature upgrading. J Chem Eng Jpn. 1996;29:119–25.
11. Kyaw K, Kubota M, Watanabe F, Matsuda H, Hasatani M. Study of carbonation of CaO for high temperature thermal energy storage. J Chem Eng Jpn. 1998;31:281–4.

12. Lin SY, Suzuki Y, Hatano H, Harada M. Developing an innovative method, HyPr-RING, to produce hydrogen from hydrocarbons. Energy Convers Manage. 2002;43:1283–90.
13. Lee DK, Baek IH, Yoon WL. Modeling and simulation for the methane steam reforming enhanced by in situ CO_2 removal utilizing the CaO carbonation for H-2 production. Chem Eng Sci. 2004;59:931–42.
14. Ryden M, Ramos P. H_2 production with CO_2 capture by sorption enhanced chemical-looping reforming using NiO as oxygen carrier and CaO as CO_2 sorbent. Fuel Process Technol. 2012;96:27–36.
15. Bouquet E, Leyssens G, Schönnenbeck C, Gilot P. The decrease of carbonation efficiency of CaO along calcination-carbonation cycles: experiments and modeling. Chem Eng Sci. 2009;64:2136–46.
16. Alvarez D, Abanades JC. Determination of the critical product layer thickness in the reaction of CaO with CO_2. Ind Eng Chem Res. 2005;44:5608–15.
17. Alvarez D, Abanades JC. Pore-size and shape effects on the re-carbonation performance of calcium oxide submitted to repeated calcination/recarbonation cycles. Energy Fuels. 2005;19:270–8.
18. Abanades JC, Alvarez D. Conversion limits in the reaction of CO_2 with lime. Energy Fuels. 2003;17:308–15.
19. Grasa GS, Abanades JC, Alonso M, Gonzales B. Reactivity of highly cycled particles of CaO in a carbonation/calcinations loop. Chem Eng J. 2008;137:561–7.
20. Barker R. The reversibility of the reaction $CaCO_3 \leftrightarrow CaO + CO_2$. J Appl Chem Biotechnol. 1973;23:733–42.
21. Bhatia SK, Perlmutter DD. Effect of the product layer on the kinetics of the CO_2-lime reaction. AIChE J. 1983;29:79–86.
22. Lee DK. An apparent kinetic model for the carbonation of calcium oxide by carbon dioxide. Chem Eng J. 2004;100:71–7.
23. Sun P, Grace JR, Lim CJ, Anthony EJ. Determination of intrinsic rate constants of the $CaO-CO_2$ reaction. Chem Eng Sci. 2008;63:47–56.
24. Sun P, Grace JR, Lim CJ, Anthony EJ. A discrete pore size distribution based gas-solid model and its application to the $CaO + CO_2$ reaction. Chem Eng Sci. 2008;63:57–70.
25. Li Z, Sun H, Cai N. Rate equation theory for the carbonation reaction of CaO with CO_2. Energy Fuels. 2012;26:4607–16.
26. Pijolat M, Soustelle M. Experimental tests to validate the rate-limiting step assumption used in the kinetic analysis of solid-state reactions. Thermochim Acta. 2008;478:34–40.
27. Barret P. Cinétique hétérogène. Paris: Gauthier-Villars; 1973.
28. Delmon B. Introduction à la cinétique hétérogène, Publications de l'institut français du pétrole. Paris: Ed. Technip; 1969.
29. Nikulshina V, Gálvez M, Steinfeld A. Kinetic analysis of the carbonation reactions for the capture of CO_2 from air via the $Ca(OH)_2$–$CaCO_3$–CaO solar thermochemical cycle. Chem Eng J. 2007;129:75–83.
30. Rouquerol F, Rouquerol J, Sing KSW. Adsorption by powders and porous solids: principles, methodology and applications. San Diego: Academic press; 1999.
31. Pijolat M, Favergeon L, Soustelle M. From the drawbacks of the Arrhenius-$f(\alpha)$ rate equation towards a more general formalism and new models for the kinetic analysis of solid–gas reactions. Thermochim Acta. 2011;525:93–102.
32. Soustelle M. Heterogenous kinetics handbook. London: Wiley-ISTE; 2010.
33. Pijolat M, Valdivieso F, Soustelle M. Experimental test to validate the rate equation "$d\alpha/dt = kf(\alpha)$" used in the kinetic analysis of solid state reactions. Thermochim Acta. 2005;439:86–93.
34. Favergeon L. PhD thesis, Ecole Nationale Supérieure des Mines. Saint-Etienne: 2006.
35. Brun C, Valdivieso F, Pijolat M, Soustelle M. Reduction by hydrogen of U_3O_8 into UO_2: nucleation and growth, influence of hydration. Phys Chem Chem Phys. 1999;1:471–7.
36. Burgers WG, Groen LJ. Mechanism and kinetics of the allotropic transformation of tin. Discuss Faraday Soc. 1957;23:183–95.
37. Mess D, Sarofim AF, Longwell JP. Product layer diffusion during the reaction of calcium oxide with carbon dioxide. Energy Fuels. 1999;13:999–1005.